Available on CMS information server

CMS NOTE 2006/004

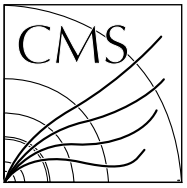

The Compact Muon Solenoid Experiment

CMS Note

Mailing address: CMS CERN, CH-1211 GENEVA 23, Switzerland

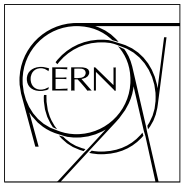

19 January 2006

TeV electron and photon saturation studies

B. Clerbaux, T. Mahmoud

ULB, Université Libre de Bruxelles, Bruxelles, Belgium

C. Collard

LLR, Ecole Polytechnique, Palaiseau, France

M.-C. Lemaire

SPP/DAPNIA, C.E. Saclay,France

V. Litvin

CALTECH, California Institute of Technology, Pasadena, California, USA

Abstract

An algorithm has been developed to correct for the saturation of the electromagnetic calorimeter electronics for electrons and photons with energies of several TeV. These corrections are important for the study of new heavy resonances decaying to electron or photon pairs.

1 Introduction

The discovery potential for heavy resonances with masses of several TeV/c^2 is studied in CMS, in the framework of searches for new physics. The electron and photon pair decay channels [1] [2] are particularly promising due to the very efficient electromagnetic calorimeter (ECAL) in CMS.

For such very energetic electrons and photons, saturation occurs in the ECAL electronics because of the limited dynamical range of the Multi-Gain-Pre-Amplifier [3]. From 2004 test beam data analysis, the saturation threshold has been established to be at 1.7 TeV in the barrel and 3.0 TeV in the endcaps.

This note presents a method to correct the central crystal energy of an electromagnetic shower in the barrel in the saturation regime. The method is based on the energy deposit in crystals surrounding the saturated crystal, using the two-dimensional (2D) profile of the electromagnetic shower.

Section 2 describes the calibration samples and the electron and photon shower characteristics. The saturation correction is presented in Section 3. The last section shows a comparison with a previous saturation correction proposed in [1].

2 Calibration samples

For this study, electron and photon calibration samples have been generated at fixed energy E and also at fixed transverse momentum p_t, with a flat pseudorapidity η distribution in the range $-2.5 < \eta < 2.5$. The primary vertex spread in the z-axis is included. The different samples are given in Table 2. The files were generated using the OSCAR (version 365) and ORCA (version 873) programs (GEANT 4 based simulation programs for CMS). In the barrel fiducial region ($|\eta| < 1.442$), electrons and photons are reconstructed in the ECAL as "super-clusters" using the "Hybrid algorithm" [4]. The reconstructed super-cluster with the highest energy is considered as the one from the electron or photon. In the super-cluster, the crystal with the highest energy deposit is taken as the central crystal, and the saturation study is performed using the information of the energy deposit in the 5×5 array of crystals around the central crystal. No saturation is introduced at the simulation level in order to study the different crystal energy correlations.

Figure 1 represents a 5×5 crystal array in the (η, Φ) plane, E_1 is the energy of the central (hatched) crystal, E_9 is the energy in the 3×3 cells, E_{25} is the energy in the 25 cells. The calibration sample distributions of E_1, E_9 and E_{25} are presented in Fig. 2 for fixed E and fixed p_t, in the case of electrons. The E_1 distribution for the fixed E samples are characterized by a large tail toward small values, mainly due to the variation of the impact position of the electron in the central crystal: when the electron impact position is situated at the center of the crystal, E_1 is high, whereas in case of an impact position at the edge of the crystal, E_1 is decreased (down to a lower limit due to the fact that the relevant crystal must remain the one with the highest energy deposit). The event to event fluctuation of the shower profile is a much weaker effect (see Section 3).

The effect of the impact position variation is recovered in the 3×3 array energy deposit E_9. The 5×5 array energy deposit E_{25} is smaller than the nominal energy by typically around 5%, mainly due to two effects: the incomplete containment of the shower in the 5×5 array, and the leakage in the HCAL behind the super-cluster. The fixed p_t calibration samples present the same features (see Fig. 2(b), (d) and (f)), together with a tail at high energy, coming from electrons with higher η.

The distributions are thus normalized to the E_{25} energy: the ratio E_1/E_{25} and E_9/E_{25} are given in Fig. 3 and Fig. 4, in the case of electrons and photons, respectively. Whereas the E_1, E_9 and E_{25} distributions for fixed E and fixed p_t are different, their ratios E_1/E_{25} and E_9/E_{25} are comparable, with similar means and widths. The ratio for the different fixed E and fixed p_t samples overlay nicely, indicating that at these energies the shower profiles are very

Table 1: Electron and photon calibration files with fixed energy and fixed transverse momentum. Each file contains 20000 simulated events.

Electrons (energies in GeV- p_t in GeV/c)								
fixed p_t	250	750	1000	1800				
fixed E	750	1000	1500	2000	2500	3000	3500	4000
Photons (energies in GeV- p_t in GeV/c)								
fixed p_t	250	750	1000	1800				
fixed E	750	1000	1500	2000	2500	3000	3500	4000

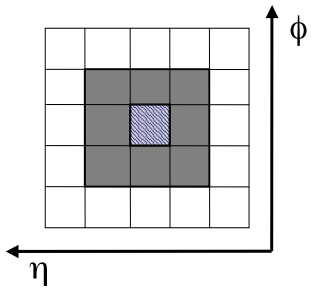

Figure 1: Representation of the 5 × 5 crystal array in the (η, Φ) plane, E_1 is the energy of the central (hatched) crystal, E_9 is the energy in the 3 × 3 cells, E_{25} is the energy in the 25 cells.

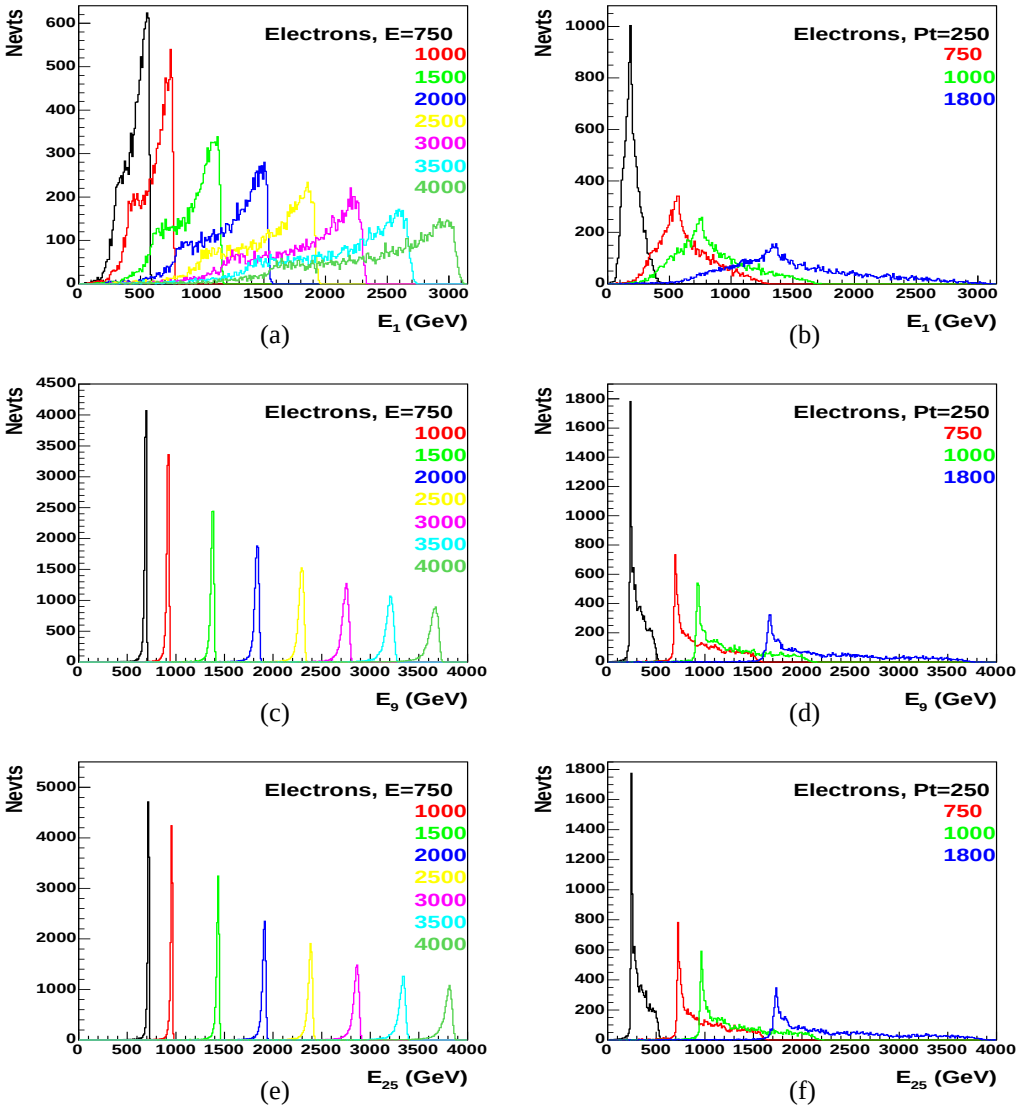

Figure 2: Distributions of E_1, E_9 and E_{25} for fixed E electron samples (figures (a), (c) and (e) respectively) and fixed p_t electron samples (figures (b), (d) and (f) respectively); energies are in GeV and p_t in GeV/c.

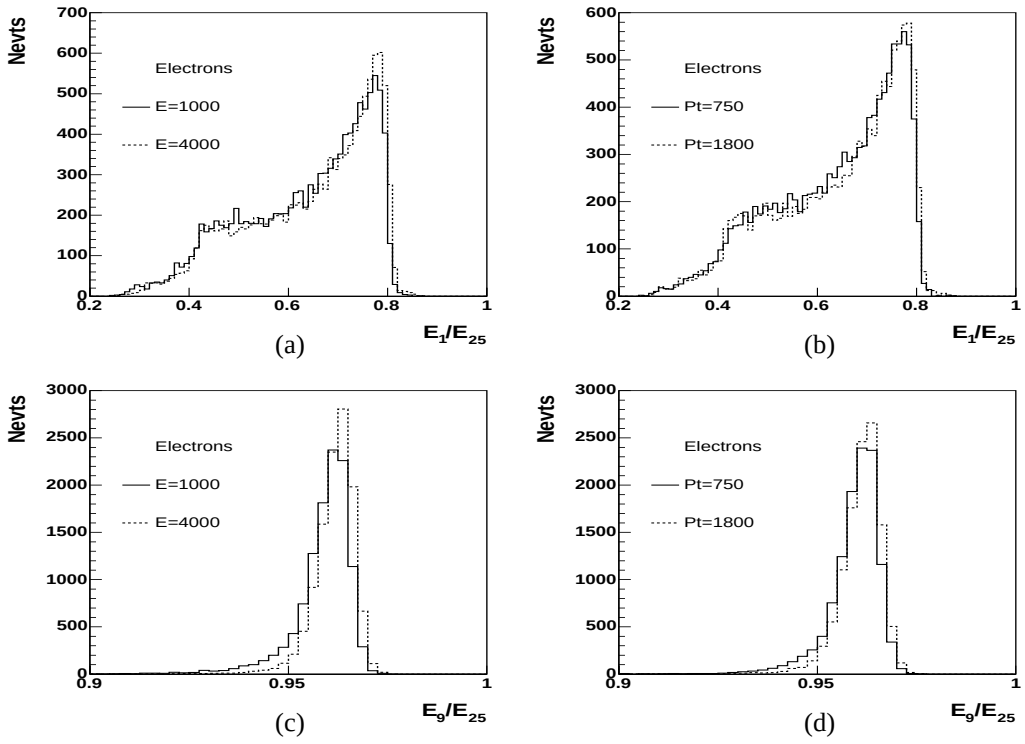

Figure 3: Distributions of the ratios E_1/E_{25} and E_9/E_{25} for electrons with fixed E (figures (a) and (c) respectively) and with fixed p_t (figures (b) and (d) respectively); energies are in GeV and p_t in GeV/c.

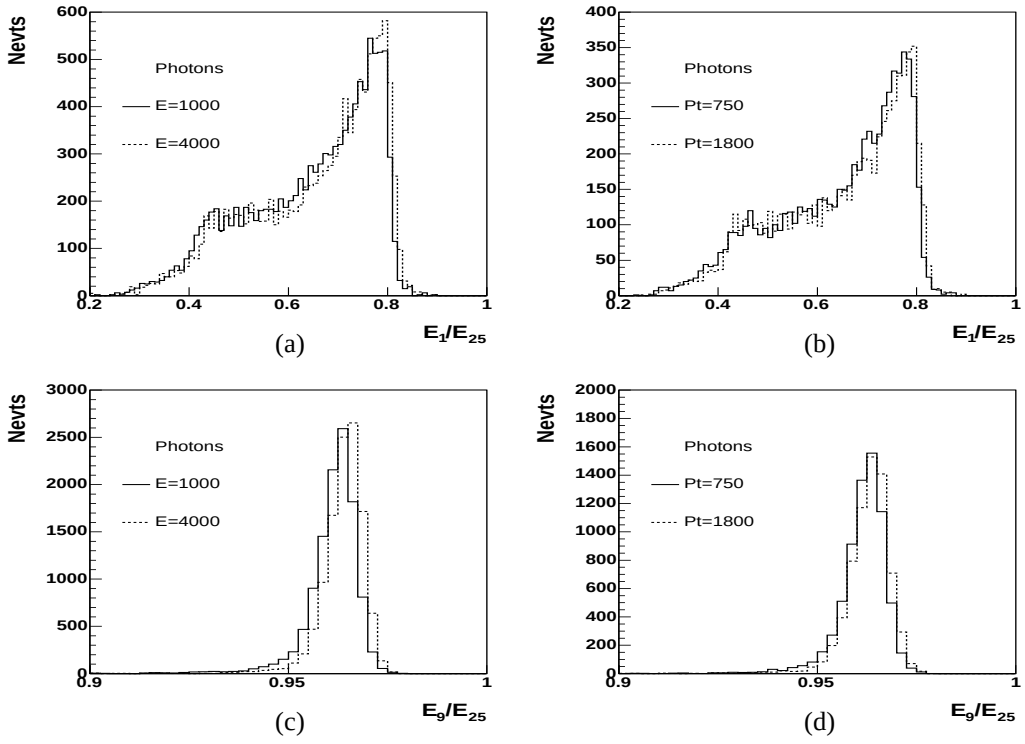

Figure 4: Distributions of the ratios E_1/E_{25} and E_9/E_{25} for photons with fixed E (figures (a) and (c) respectively) and with fixed p_t (figures (b) and (d) respectively); energies are in GeV and p_t in GeV/c.

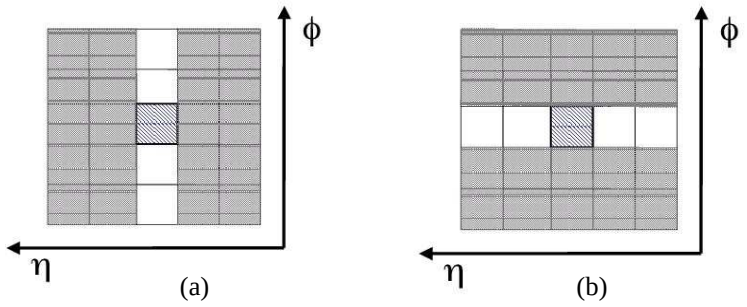

Figure 5: Representation of the 5×5 crystal array in the (η, Φ) plane: (a) description of $\Sigma_{\rm left}$ and $\Sigma_{\rm right}$ variables; (b) description of $\Sigma_{\rm top}$ and $\Sigma_{\rm bottom}$.

similar, although one notices that the energy fraction is slightly higher at highest energy.

It is also observed that the distributions for electrons and photons are similar in shape, with however a small shift towards a lower ratio in the case of electrons. This is explained by the small widening of the measured electron showers due to Bremsstrahlung emission convoluted with the effect of the CMS magnetic field.

In the method presented here, the E_1 energy is estimated using both the energy deposit in the other 24 crystals of the array, and an estimation of the electron/photon impact position in the central crystal.

3 The electronics saturation correction

Let us consider the 5×5 array in the (η, Φ) plane surrounding the struck crystal. The horizontal (X) and vertical (Y) variables are defined as the following:

$$X = \ln(\frac{\Sigma_{\rm right}}{\Sigma_{\rm left}}) \quad , \quad Y = \ln(\frac{\Sigma_{\rm top}}{\Sigma_{\rm bottom}}) \tag{1}$$

where $\Sigma_{\rm left}$ ($\Sigma_{\rm right}$) is the sum of the energy deposit in the 10 crystals located at the left (right) side of the central crystal as shown in Fig. 5(a), and $\Sigma_{\rm top}$ ($\Sigma_{\rm bottom}$) is similarly the energy deposit in the 10 top (bottom) crystals, as shown in Fig. 5(b).

As an example, for fixed electron energy $E = 4000$ GeV, the $|X|$ and $|Y|$ values for each event are presented in Fig. 6. For most events, small values of $|X|$ and $|Y|$ are observed, i.e. rather symmetric energy deposits. Larger values of $|X|$ and $|Y|$ are attributed to impact positions closer to the edge of the central crystal.

The effect of the variation of the energy deposit in the central crystal as a function of the position of the incoming electron or photon gives a similar pattern in $|X|$ and $|Y|$. The Bremsstrahlung emission effect is typically in the Φ direction, and is expected to affect mostly the $|Y|$ variable. Figure 7 helps to visualize the dependence of the ratio E_1/E_{25} on the variables $|X|$ and $|Y|$. Events with a large imbalance between the left and right sides in the 5×5 array, i.e. at large $|X|$, are characterized by a lower E_1/E_{25} ratio. The same is observed for the $|Y|$ dependence, with a smaller E_1/E_{25} ratio at high $|Y|$ value, due to the above quoted Bremsstrahlung effect.

The effect of the shower position is also visible in Fig. 8, where the E_1/E_{25} ratio is given for three different bins in the $(|X|, |Y|)$ plane: the bin $X = [0.00, 0.33]$ and $Y = [0.00, 0.33]$, the bin $X = [0.00, 0.33]$ and $Y = [1.33, 1.67]$, and the bin $X = [0.00, 0.33]$ and $Y = [2.67, 3.00]$. One observes that the event to event fluctuation of the shower profile (the width in each of the three plots of Fig. 8) is much smaller than the effect due to the shower position in the central crystal, as estimated by the Φ and η asymmetries in the energy deposit (comparing for example the mean values of Fig. 8(a) and (c)). In each of the bins, a Gaussian fit is performed on the E_1/E_{25} ratio, and the mean value of the fit is reported in Fig. 9.

The proposed method thus uses the correlation between the E_1/E_{25} ratio and the $|X|$ and $|Y|$ variables: a two-dimensional fit of this dependence is performed with a function:

$$F(X, Y) = a + b(e^{cX^2} + e^{dY^2}) + eX^2 + fY^2. \tag{2}$$

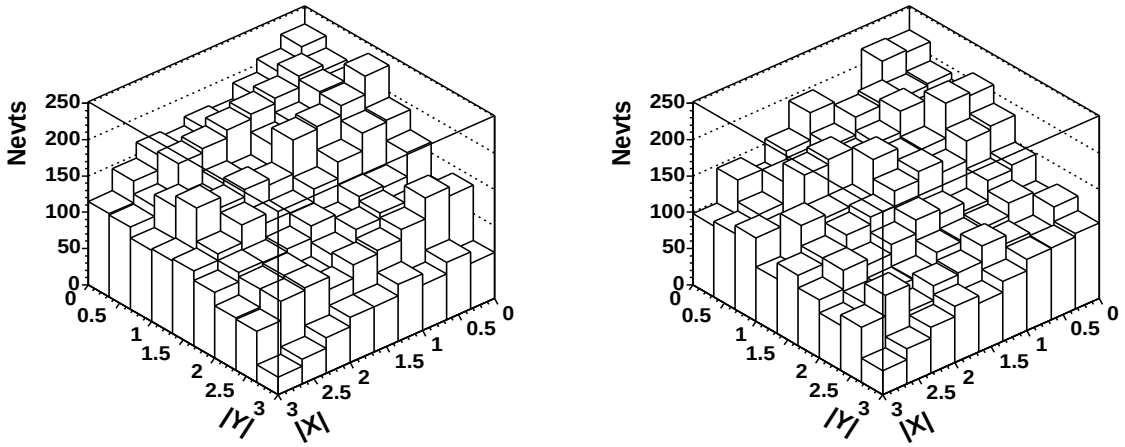

(a) (b)

Figure 6: Number of events in 9×9 bins in the $|X|$ and $|Y|$ plane, where X and Y are defined in Eq. 1, for electrons (a) and photons (b) with $E = 4000$ GeV.

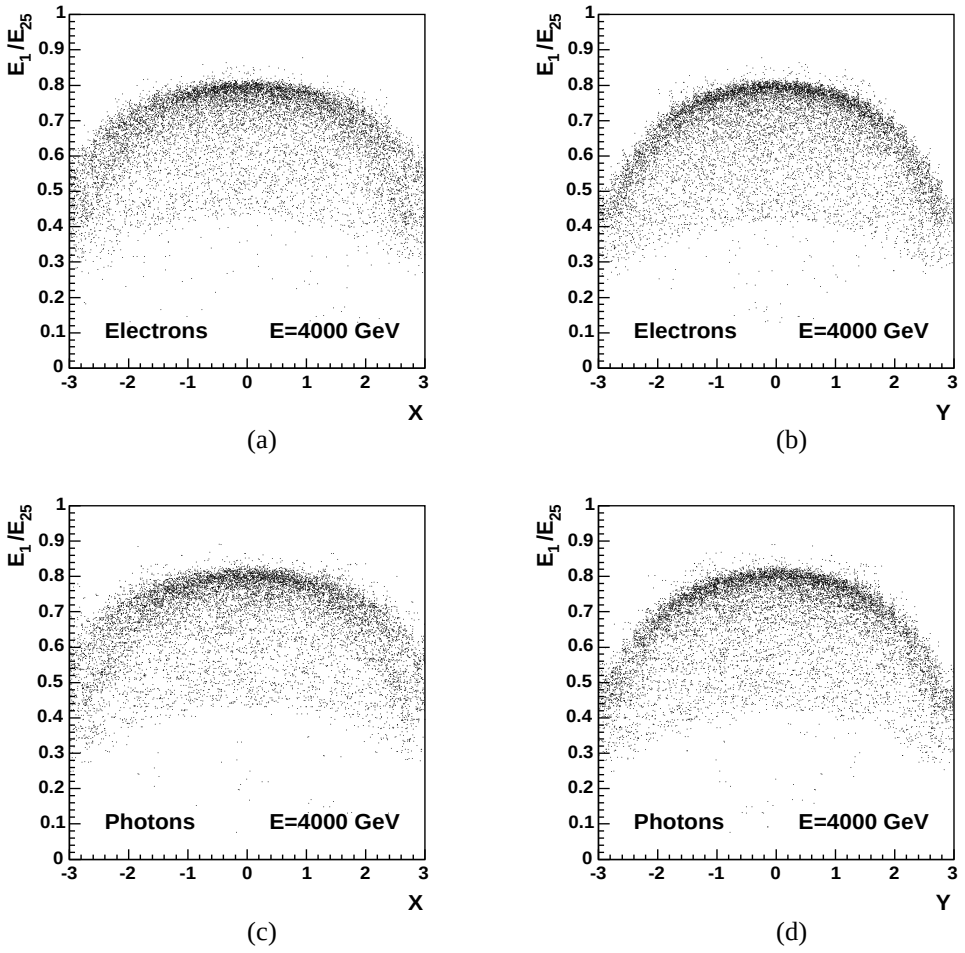

(a) (b)

(c) (d)

Figure 7: Distributions of the ratio E_1/E_{25} as a function of the variable X for electrons (a) and photons (c), and as a function of the variable Y for electrons (b) and photons (d), for $E = 4000$ GeV.

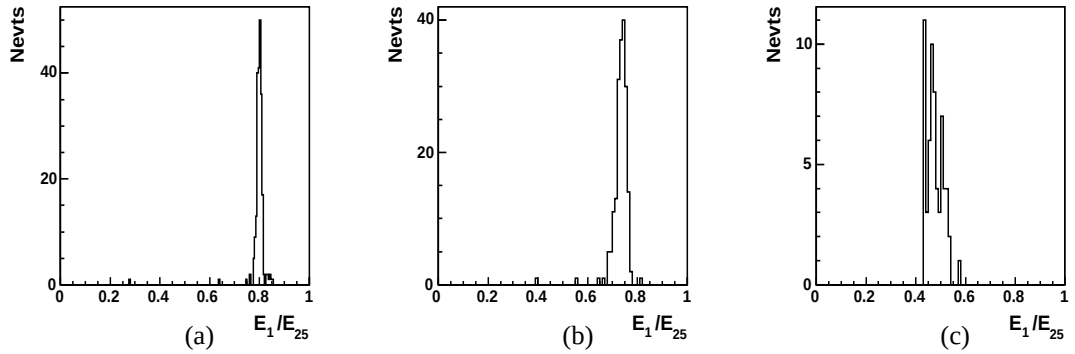

Figure 8: Distributions of the ratio E_1/E_{25} in three different bins in the X and Y plane: (a) $X = [0.00, 0.33]$ and $Y = [0.00, 0.33]$; (b) $X = [0.00, 0.33]$ and $Y = [1.33, 1.67]$; (c) $X = [0.00, 0.33]$ and $Y = [2.67, 3.00]$; for electrons with $E = 4000$ GeV.

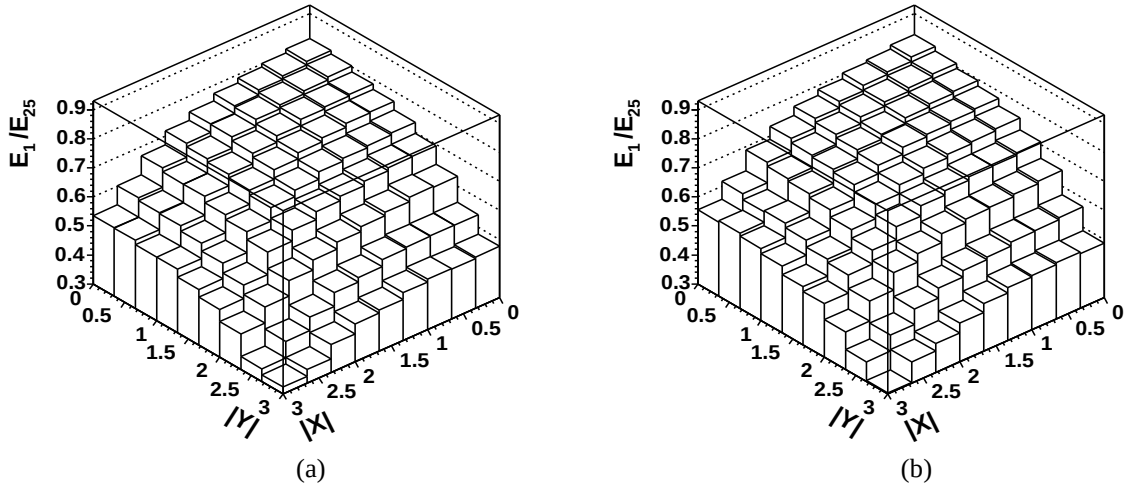

Figure 9: Distribution of the E_1/E_{25} ratio as a function of $|X|$ and $|Y|$, for electrons (a) and photons (b) with $E = 4000$ GeV.

The fitted function is displayed in Fig. 10 for $E = 4000$ GeV. The corresponding residual distribution, defined as the difference between the E_1/E_{25} ratio and the function of Eq. 2, divided by the E_1/E_{25} ratio, is given in Fig. 11. The residuals are lower than 4% in most of the $|X|$ and $|Y|$ plane. Because the electron and photon shower profile is very slightly energy dependent, the fitted function of Eq. 2 is also nearly energy independent. This can be seen in Fig. 12 which represents the fitted function in the case of X=Y, for five fixed electron energies: $E = 2000$, 2500, 3000, 3500 and 4000 GeV.

The 2D method to correct for saturation is the following. The E_1/E_{25} ratio is estimated for the particular $|X|$ and $|Y|$ event values, using the parameters of function 2 obtained for $E = 3500$ GeV. From the E_1/E_{25} ratio, the corrected E_{25} is reconstructed using the formula: $E_{25} = E_{24}/(1 - F(X, Y))$, where $E_{24} = E_{25} - E_1$.

Figure 13 shows the estimated value of the 5×5 crystal energy E_{25} using the correction method for the saturation divided by the nominal E_{25}, for E=3000, 3500 and 4000 GeV electrons and photons. The highest energy files are used as only events with saturation of the central crystal in the barrel are considered (see Fig. 2(a) with $E_1 > 1.7$ TeV).

One observes that the distributions are peaked around 1 and are reasonably symmetric (taking into account the constraint due to the choice of the crystal with the highest energy deposit). The values of the mean and the RMS of the distributions are given in Table 2. Gaussian distributions are fitted to these data, for the ratio in the range $[0.85 - 1.15]$, i.e. about 85% of the events. The corresponding mean values and standard deviations are also given in Table 2, showing that the corrected values peak at 1.00 within less than 1% and that the resolution of the method is about 7% for electrons and 8% for photons. It should be reminded that these results apply for showers expected to saturate the central crystal.

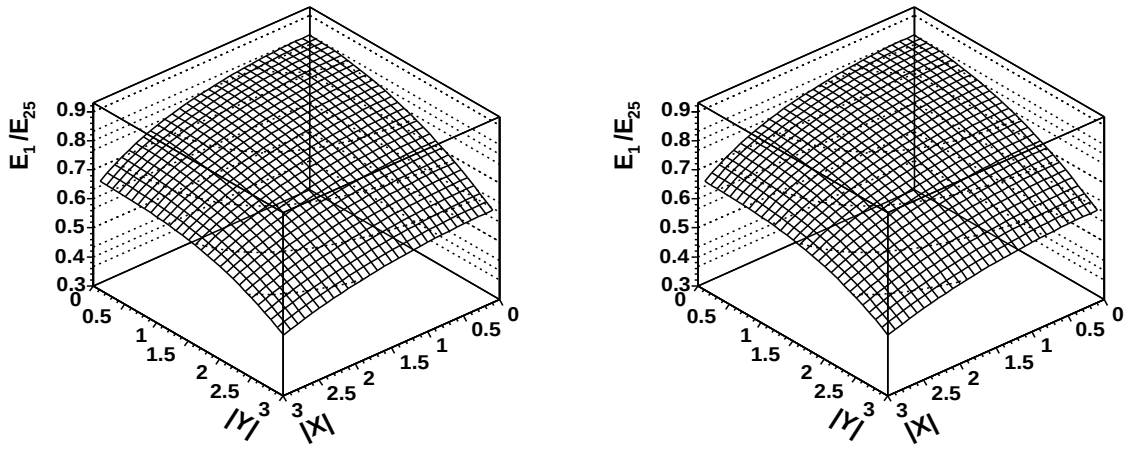

(a) (b)

Figure 10: Fitted function (see Eq.2) of the E_1/E_{25} ratio as a function of $|X|$ and $|Y|$ for electrons (a) and photons (b) with $E = 4000$ GeV.

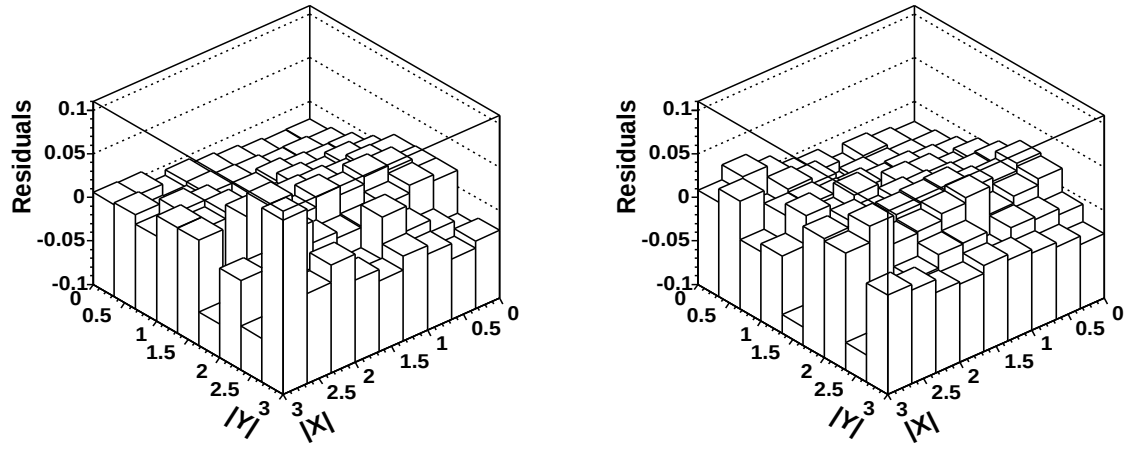

(a) (b)

Figure 11: Distribution of the residuals (as defined in the text) as a function of $|X|$ and $|Y|$ for electrons (a) and photons (b) with $E = 4000$ GeV.

Table 2: Comparison between electron and photon E_{25} resolution after the 2D method for saturation correction: mean and RMS of the $E_{25}^{\rm cor}/E_{25}$ distribution, as well as mean (μ) and standard deviation (σ) of the Gaussian fits, for fixed E samples of 3000, 3500 and 4000 GeV.

	Electrons				Photons			
E (GeV)	mean	RMS	μ	σ	mean	RMS	μ	σ
3000	1.018	0.086	1.009	0.074	1.011	0.095	1.006	0.084
3500	1.019	0.092	1.005	0.073	1.008	0.104	0.999	0.083
4000	1.023	0.099	1.006	0.076	1.015	0.116	0.999	0.084

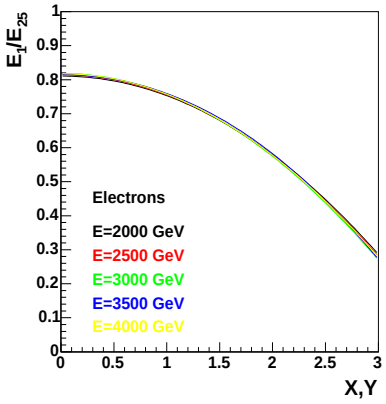

Figure 12: Fitted function (see Eq.2) of the E_1/E_{25} ratio in the case $|X| = |Y|$ for electrons with $E = 2000, 2500, 3000, 3500$, and 4000 GeV.

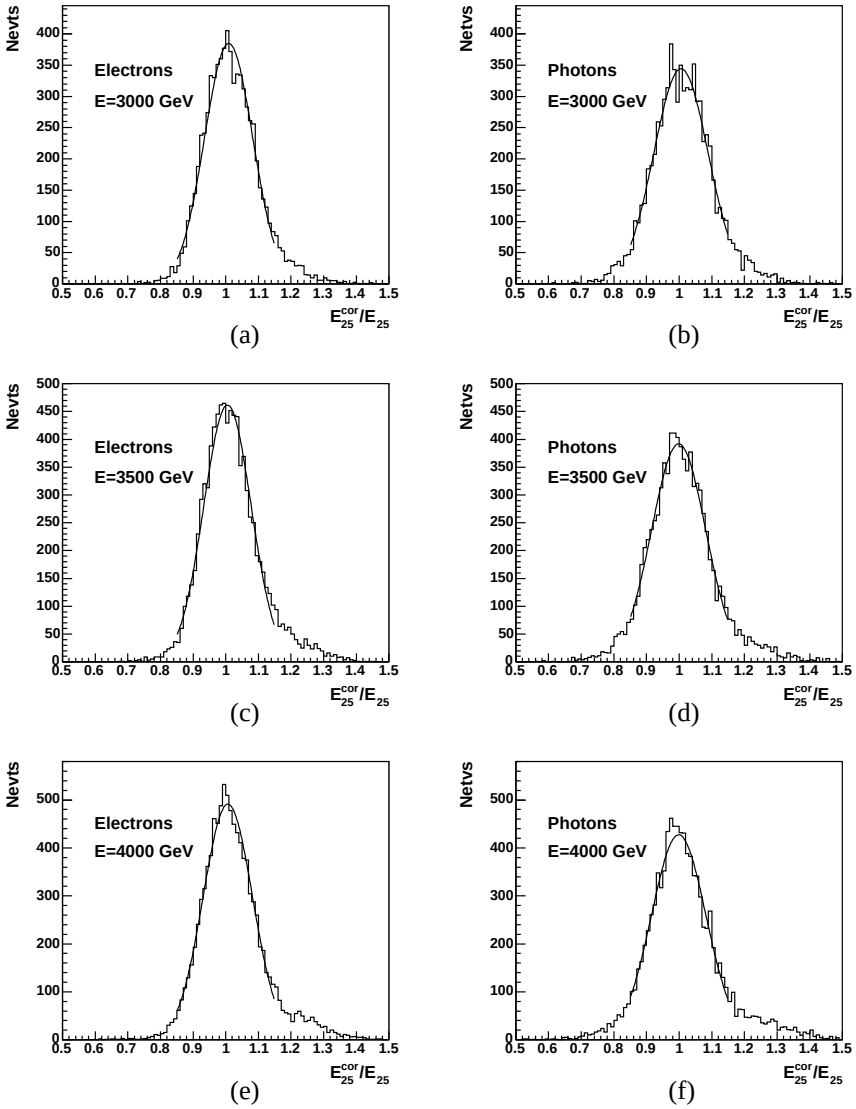

Figure 13: Distribution of $E_{25}^{\rm cor}/E_{25}$ for electrons (a), (c) and (e) and for photons (b), (d) and (f) for E=3000, 3500 and 4000 GeV, respectively.

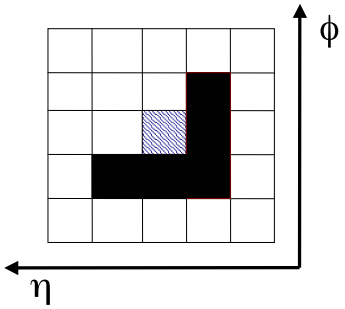

Figure 14: Representation of the 5×5 crystal array in the (η, Φ) plane, E_1 is the energy of the central (hatched) crystal, E_{25} is the energy in the 25 cells and $E_5 = E_9 - E_4$ is the energy of the 5 crystals in black.

4 Correlation between E_1 and E_5

In a previous study of saturation effects [1] using electron calibration files and the CMSIM simulation (GEANT 3 based simulation program for CMS), a correlation was observed between E_1 and E_5, the energy deposited in the least energetic corner of 5 crystals: E_5 = E_9-E_4, where E_9 is the energy of the 3×3 crystal array in the $\Phi - \eta$ plane around the central crystal and E_4 is the most energetic 2×2 crystal array in the 3×3 array. In Fig. 14, the hashed square is the central crystal with energy E_1 and E_5 is the energy of the crystals in black, in the hypothesis that E_4 is found at the top left side of the central crystal. This correlation is studied here using the calibration files described in section 2, thus extending it to photons.

Figures 15(a) and (b) show the E_1-E_5 correlation for electrons and photons generated at fixed energy and Figs. 15(c) and (d) show the correlation for the fixed p_t samples. The figures show the profile histograms, i.e. the mean values and the RMS of the E_1 distribution for different E_5 slices.

The E_1-E_5 correlation is visible in all plots. However the same E_5 value can be obtained for electrons/photons with different energies if the shower center position changes. For a given E_5 value, E_1 is smaller when the impact position is at the center of the crystal, and increases as the impact point moves to the corner opposite to the E_5

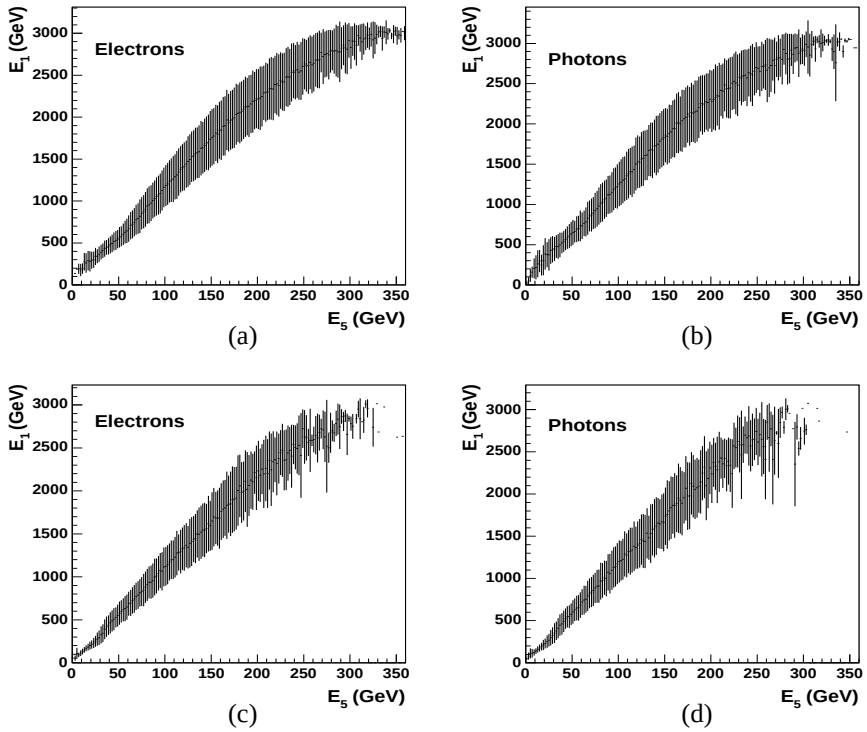

Figure 15: Correlation between E_1 and E_5: for electrons (a) and photons (b) generated at fixed energy; for electrons (c) and photons (d) generated at fixed p_t.

array. The E_1-E_5 correlation then suffers from a large spread. As an example, a fixed E_5 value of 200 GeV may come from a 1700 GeV electron with a central impact position, or from a 2500 GeV electron with a non-central impact position. (The apparent decrease of the RMS spread at large E_5 values is due to the limited range of generated energies, $E \leq 4000$ GeV.)

To fit the E_1-E_5 linear dependence, the E_5 spectra for different E_1 slices are fitted with Gaussian functions. The distributions of the E_1 slice center as a function of the E_5 Gaussian mean values are shown in Fig. 16. A fit restricted to $20 < E_5 < 100$ GeV gives $E_1 = a\ E_5$ with $a = 12.1 \pm 0.2$ for electrons and $a = 12.6 \pm 0.2$ for photons. The results for electrons are compatible with the one obtained in case of the CMSIM detector simulation of [1]. The slope in the case of electrons is slightly lower than for photons, showing that the energy fraction E_5/E_1 is slightly larger (5%) for electrons than for photons. This slightly wider profile of electron showers is attributed to the effect of Bremsstrahlung emission in the CMS material.

To estimate the resolution of this correction (labeled as the 1D method), the same procedure is followed as for the 2D method described at the end of section 3. Table 4 gives the mean and RMS of the $E_{25}^{\rm cor}/E_{25}$ distributions as well as the mean and the standard deviations of the Gaussian fits (on the range $[0.85 - 1.15]$, i.e. about 80% of the events). The distributions peak at 1.00 within less than 1% and the resolution is about 12% and 13% for electrons and photons, respectively.

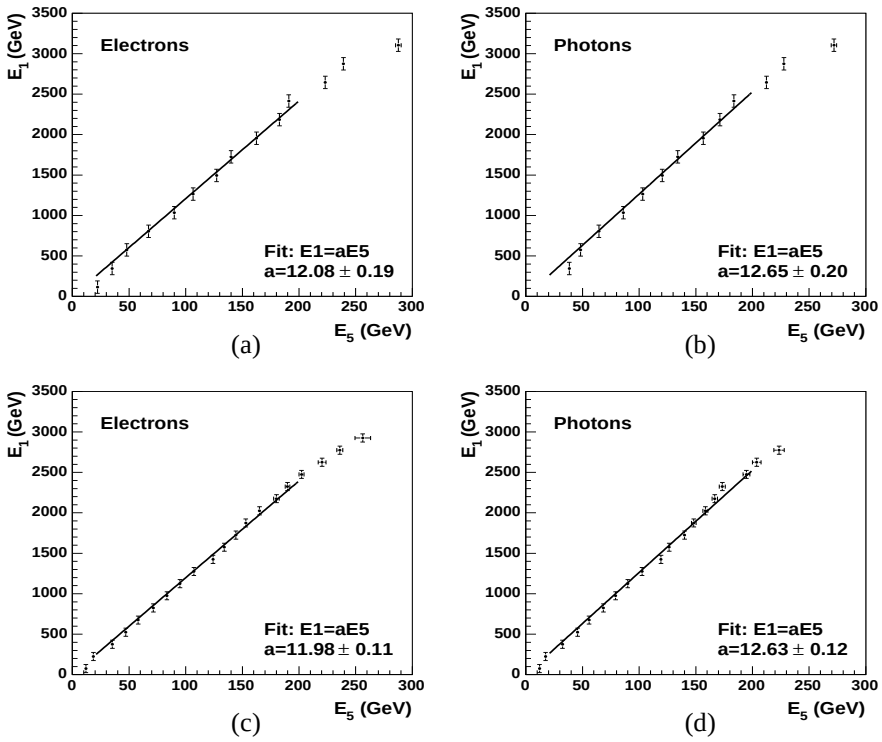

Figure 16: Linear fit of the E_1-E_5 correlation, for fixed E electrons (a) and photons (b), and for fixed p_t electrons (c) and photons (d).

Table 3: Comparison between electron and photon E_{25} resolution after the 1D method for saturation correction: mean and RMS of the $E_{25}^{\rm cor}/E_{25}$ distribution, as well as mean (μ) and standard deviation (σ) of the Gaussian fits, for fixed E samples of 3000, 3500 and 4000 GeV.

	Electrons				Photons			
E (GeV)	mean	RMS	μ	σ	mean	RMS	μ	σ
3000	1.023	0.115	1.000	0.123	1.014	0.122	0.995	0.128
3500	1.023	0.115	1.000	0.118	1.008	0.122	0.985	0.133
4000	1.025	0.117	1.005	0.120	1.010	0.126	0.992	0.127

5 Normalized 1D method

The 1D method described in the previous section can be improved by using in addition to E_5 the energy in the 24 cells around the central crystal E_{24}= E_{25} - E_1. This additional information disentangles the energy dependence (estimated with E_{24}) from the central crystal impact position dependence (estimated with E_5).

The correlation between E_1/E_{25} and E_5/E_{24} is presented in Fig. 17 for electrons and photons, using all the fixed energy files. To estimate the E_1/E_{25} and E_5/E_{24} correlation, the E_5/E_{24} spectra for different E_1/E_{25} slices are fitted with Gaussian functions.

The distribution of the E_1/E_{25} slice centers as a function of the E_5/E_{24} Gaussian mean values is shown in Fig. 18 for electrons and photons generated at fixed energy, and a fourth-order polynomial function restricted to $0.07 < E_5/E_{24} < 0.35$ is fitted to the points. As for the 2D method the fitted function is mostly energy independent in the range E=3000, 3500 and 4000 GeV, as it is shown in Fig. 19(a). A comparison of the fitted functions for electrons and the photons is given in Fig. 19(b).

The 1D-improved method to correct for saturation is then the following. The E_1/E_{25} ratio is estimated for the particular E_5 and E_{24} event values, using the fitted fourth-order polynomial function described above. From the E_1/E_{25} ratio, the corrected E_{25} is reconstructed using the formula: $E_{25} = E_{24}/(1 - F(E_5/E_{24}))$.

Similarly to previous section, the E_{25} resolution of the 1D-improved method is estimated. Table 5 gives the mean and RMS of the $E_{25}^{\rm cor}/E_{25}$ distributions as well as the mean and the standard deviations of the Gaussian fits. The resolution is about 8% and 9% for electrons and photons, respectively. These resolutions are in between the ones from the 1D and 2D methods described in section 4 and section 3, respectively.

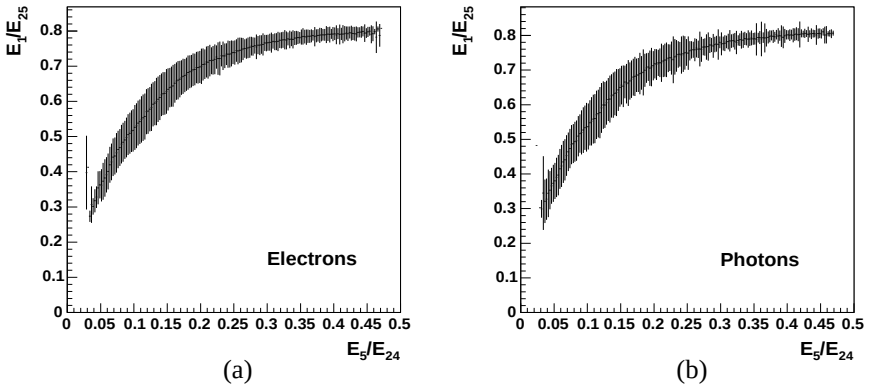

Figure 17: Correlation between E_1/E_{25} and E_5/E_{24}: for electrons (a) and photons (b) generated at fixed energy.

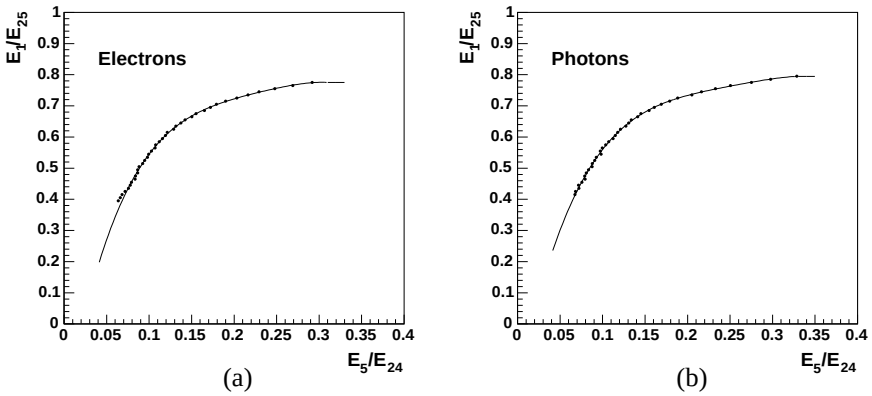

Figure 18: Fit of the E_1/E_{25}-E_5/E_{24} correlation using a fourth-order polynomial function, for fixed E electrons (a) and photons (b).

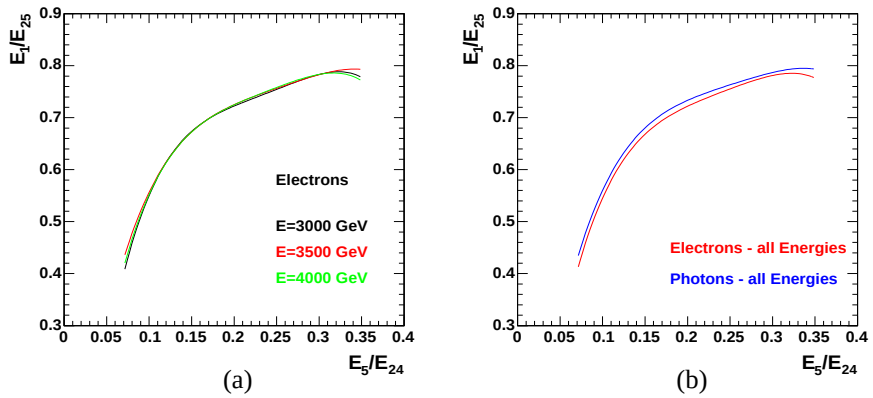

Figure 19: Comparison of the E_1/E_{25}-E_5/E_{24} correlations for different energies (a) and between electrons and photons (b).

Table 4: Comparison between electron and photon E_{25} resolution after the 1D-improved method for saturation correction: mean and RMS of the $E_{25}^{\rm cor}/E_{25}$ distribution, as well as mean (μ) and standard deviation (σ) of the Gaussian fits, for fixed E samples of 3000, 3500 and 4000 GeV.

	Electrons				Photons			
E (GeV)	mean	RMS	μ	σ	mean	RMS	μ	σ
3000	1.017	0.094	1.003	0.076	1.013	0.101	1.002	0.084
3500	1.022	0.110	1.001	0.083	1.015	0.117	0.998	0.087
4000	1.021	0.116	0.999	0.085	1.014	0.125	0.996	0.096

The use of the additional information (E_{24}) improves the resolution on E_{25} considerably, compared to the one obtained with the 1D method. Nevertheless, the 1D-improved method has a worse resolution than the 2D method. Indeed, the E_5 variable is less powerful in estimating the electron/photon impact position in the central crystal compared to the use of the X and Y variables. Figure 20 shows the resolution on E_{25} using the 1D, the 1D-improved and the 2D correction methods for the saturation.

6 Conclusions

According to the analysis of the 2004 test beam data, the central crystal in an electromagnetic shower in the barrel calorimeter of CMS is expected to saturate above 1.7 TeV. To reconstruct the central crystal energy E_1, the incoming electron/photon energy dependence has to be disentangled from the energy variation coming from the different possible impact position of the electron/photon in the central crystal. A two-dimensional method is proposed to correct the central crystal energy in the saturation regime. It uses the total energy deposit and the (η, Φ) profile of the shower in the 5×5 crystal array surrounding the central crystal. The ratio of the reconstructed over the true energy for showers expected to show saturation of the central crystal peaks at 1.00 ± 0.01, with a resolution of the order of 7% and 8% for electrons and photons, respectively, in the energy range where they saturate. A previous method based on the E_1-E_5 correlation reconstructs the saturated cell energy with a resolution of about 12% and 13% for electrons and photons, respectively. An improved version of this method gives a resolution of about 8% and 9% for electrons and photons, respectively.

Acknowledgments

C. Collard and T. Mahmoud acknowledge the financial support provided through the European Community's Human Potential Programme under contract HPRN-CT-2002-00326, PRSATLHC, and through the Pôle d'Attraction Inter Universitaire (PAI) in Belgium, respectively.

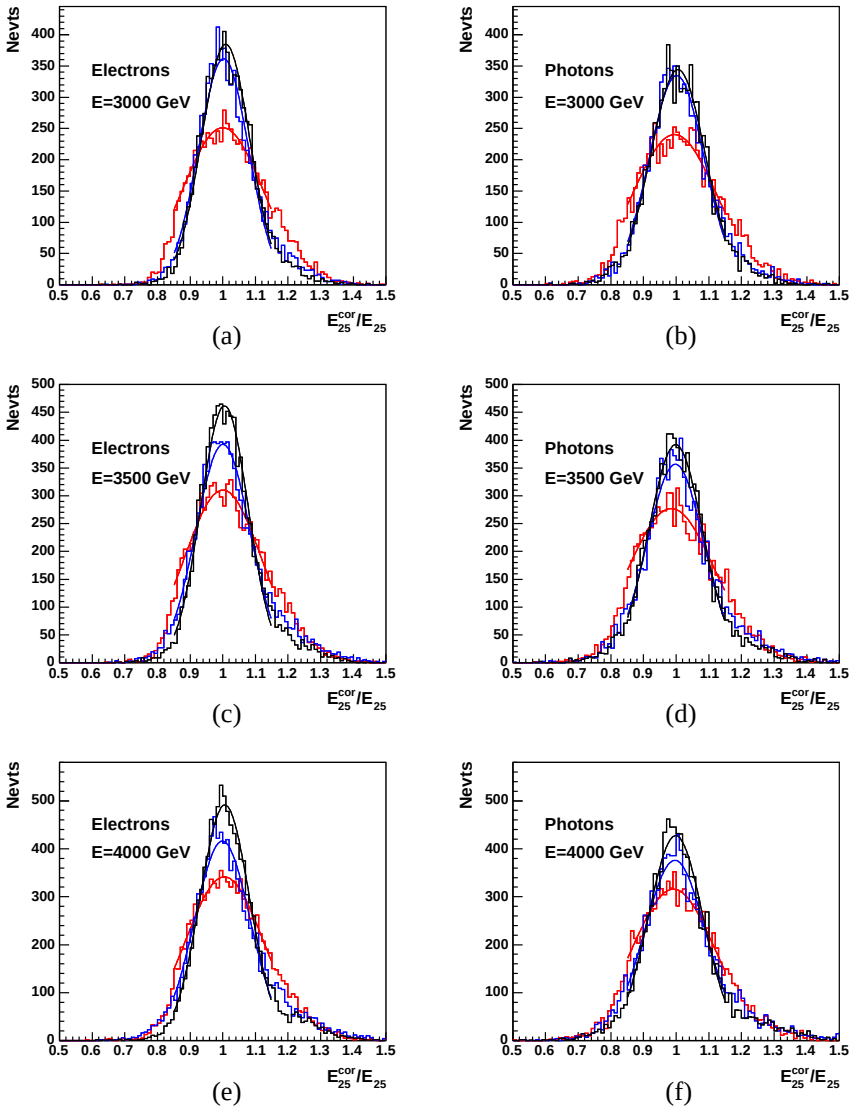

Figure 20: Distribution of $E_{25}^{\rm cor}/E_{25}$ for the 1D (lower histogram and curve), 1D-improved (middle histogram and curve) and 2D (upper histogram and curve) saturation correction methods, for electrons (a), (c) and (e), and for photons (b), (d) and (f), for E=3000, 3500 and 4000 GeV, respectively.

References

[1] C. Collard and M.-C. Lemaire, *"Search with the CMS detector for Randall-Sundrum excitations of gravitons decaying into electron pairs"*, Eur. Phys. J. **C40N5**(2005)15.

[2] C. Collard, M.-C. Lemaire, P. Traczyk, G. Wrochna, *"Prospects for Study of Randall-Sundrum Gravitons in the CMS Experiment"*, **CMS NOTE 2002-050**.

[3] M. Raymond, J. Crooks, M. French and G. Hall, *"The MGPA Electronic Calorimeter Readout Chip for CMS"*, Proceeding of the 2003 LECC Conference, **CERN-2003-006**.

[4] E. Meschi, T. Montero, C. Seez and P. Vikas, *"Electron Reconstruction in the CMS Electromagnetic Calorimeter"*, **CMS NOTE 2001-034**.